

RESEARCH ARTICLE | APRIL 24 2024

Dual-comb interchanging absolute distance measurement with non-ambiguity range extension

Xiaodong Shao ; Hainian Han  ; Yu Yan; Junyi Ma; Chengzhi Li; Zhiyi Wei 

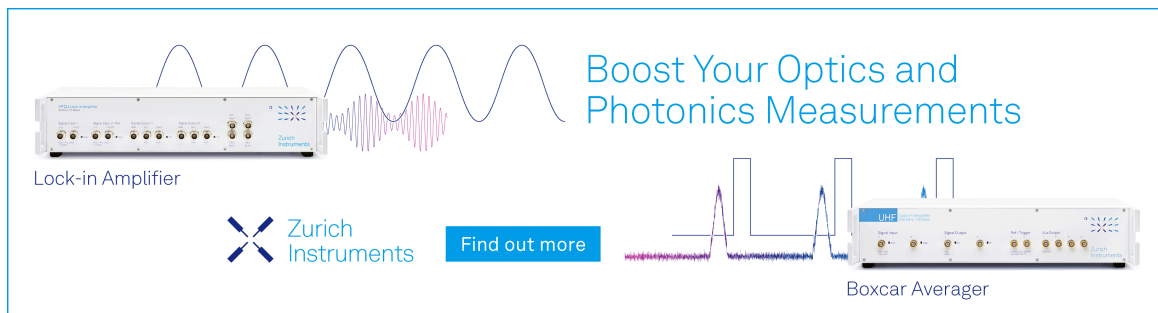


Appl. Phys. Lett. 124, 171103 (2024)

<https://doi.org/10.1063/5.0202465>



Boost Your Optics and Photonics Measurements



Lock-in Amplifier



Find out more

Boxcar Averager

Dual-comb interchanging absolute distance measurement with non-ambiguity range extension

Cite as: Appl. Phys. Lett. **124**, 171103 (2024); doi: [10.1063/5.0202465](https://doi.org/10.1063/5.0202465)

Submitted: 4 February 2024 · Accepted: 15 April 2024 ·

Published Online: 24 April 2024



View Online



Export Citation



CrossMark

Xiaodong Shao,¹ Hainian Han,^{1,2,a)} Yu Yan,¹ Junyi Ma,¹ Chengzhi Li,¹ and Zhiyi Wei^{1,2,b)}

AFFILIATIONS

¹Beijing National Laboratory for Condensed Matter Physics, Institute of Physics, Chinese Academy of Sciences, Beijing 100190, China

²Shongshan Lake Materials Laboratory, Dongguan, Guangdong 523808, China

^{a)} Author to whom correspondence should be addressed: hnhan@iphy.ac.cn

^{b)} Electronic mail: zywei@iphy.ac.cn

ABSTRACT

We demonstrate a rapid and high-precision dual-comb ranging method with a significantly extended non-ambiguity range (NAR). By reasonably setting the polarization combining and splitting of two optical combs, we can obtain two sets of interferograms of signal comb and local oscillator comb interchanging simultaneously. This method allows us to extend the NAR to tens to hundreds of kilometers without changing the repetition rate of the signal comb. With this scheme, we demonstrate a dynamic distance measurement when a moving target crosses a measurement dead zone that is 3–4 times the NAR. The standard deviation of the residual distance is $1.48 \mu\text{m}$ with a $925 \mu\text{s}$ update rate. This rapid, high-precision, and NAR extension absolute distance measurement scheme will have broad potential in various ranging applications.

© 2024 Author(s). All article content, except where otherwise noted, is licensed under a Creative Commons Attribution (CC BY) license (<https://creativecommons.org/licenses/by/4.0/>). <https://doi.org/10.1063/5.0202465>

Accurate, fast, and large-range absolute distance measurement plays a crucial role in various applications, including satellite formation flying, microelectronics equipment manufacturing, and large-scale equipment installation.^{1–3} Several high-precision absolute distance measurement schemes based on the optical frequency comb were implemented and achieved good results, owing to the good timing characteristics and the coherence of the spectrum of the optical frequency comb.^{4–8} Of these technologies, the dual-comb absolute distance measurement technology based on asynchronous optical sampling offers significant advantages, such as high measurement accuracy (nm- μm), fast update speed (μs -ms), and expandable non-ambiguity range (NAR). Thus, it has been widely studied in the past decade. It uses two optical frequency combs with slight differences in the repetition rate to scan each other to improve the accuracy of distance. The research progress in free-running dual-comb ranging,⁹ asynchronous nonlinear optical sampling,¹⁰ dead zone elimination,¹¹ microcomb range measurement,^{12,13} and non-ambiguity range (NAR) extension^{8,11} based on dual combs has further simplified the complexity of dual combs ranging and improved their application scenarios.¹⁴

When using dual combs for absolute ranging, its regular NAR is limited to $c/2n_g f_r$, where c represents the speed of light, n_g is the group refractive index of the air, and f_r is the repetition rate of the signal

comb. It has been proposed that by utilizing the Vernier effect,^{8,11} the repetition rate of the signal comb can be altered to $f_r + \Delta f_r$ to extend the non-ambiguity range. After conducting two independent measurements, it becomes possible to calculate an absolute distance greater than the NAR, and the NAR can be extended to $c/2n_g \Delta f_r$. However, altering the repetition rate of the signal comb undermines the rapid performance of dual-comb ranging. Particularly for fast-moving objects beyond regular NAR, it is impractical to change the repetition rate for two measurements. In 2014, Zhang *et al.* proposed an asynchronous nonlinear dual-comb ranging scheme that allows for simultaneous measurement of L_A and L_B , effectively reducing the influence of optical path variation on absolute distance measurement.^{15,16} Nonlinear optical sampling, however, requires a higher peak power, which restricts its application in long-distance measurements. In addition, there are several methods to extend the NAR, such as modulation of the repetition rate or amplitude,^{17,18} or the use of a tri-comb setup.^{19,20} However, these methods have increased the complexity of the ranging system to some extent.

In this study, we propose a more straightforward NAR extension dual-comb absolute ranging setup. This setup combines the advantages of rapid, high precision, and large-range measurements. This technique leverages the repetition rate difference between two combs,

allowing them to conduct distance measurements. In this process, two sets of interferograms of signal comb and local oscillator comb are obtained interchangeably. With this method, the NAR can be extended to $c/2n_g\delta f_r$, where δf_r represents the repetition rate difference between two combs. Unlike other methods, this scheme does not require the repetition rate to be altered, making it possible for rapid and real-time distance measurement. Similar schemes were also reported last year and were found to be effective in achieving dynamic precision distance measurement.^{21,22} However, they only showed displacement measurements for small-range movements of a few tens of micrometer. In our study, we provide a detailed explanation of how to use this method to determine the integer value m of regular NAR. The measurement precision of this setup is $4\ \mu\text{m}$ at $185\ \mu\text{s}$. If prolonging the integrated time to 180 ms, it will be raised to 180 nm. Notably, we demonstrate a rapid distance measurement when a moving target crosses a measurement dead zone that is 3–4 times the NAR and has a velocity of 15 mm/s. The standard deviation of the residual between the absolute distance and the linear fit lines is $1.48\ \mu\text{m}$ with a $925\ \mu\text{s}$ update rate.

The fundamental schematic is illustrated in Fig. 1(a). The system comprises two homemade ytterbium-doped fiber optical frequency combs that are based on nonlinear polarization evolution mode-locking and linear chirped pulse amplification technologies. The output spectrum from the Yb: doped fiber amplifier is depicted in Fig. 1(b), with a central wavelength of 1040 nm and a spectral width of 17 nm. After the bandpass filter, the spectra's full width at half maxima is 1.6 nm. The narrower spectrum is utilized to prevent spectral aliasing in dual-comb linear optical sampling.²³ The repetition rate is approximately 201 MHz, with a tuning range of 6 MHz by installing a translation stage under the oscillator end mirror. We use a rubidium clock that distributes synchronous signals to various devices, including signal generators, frequency synthesizers, and frequency counters.

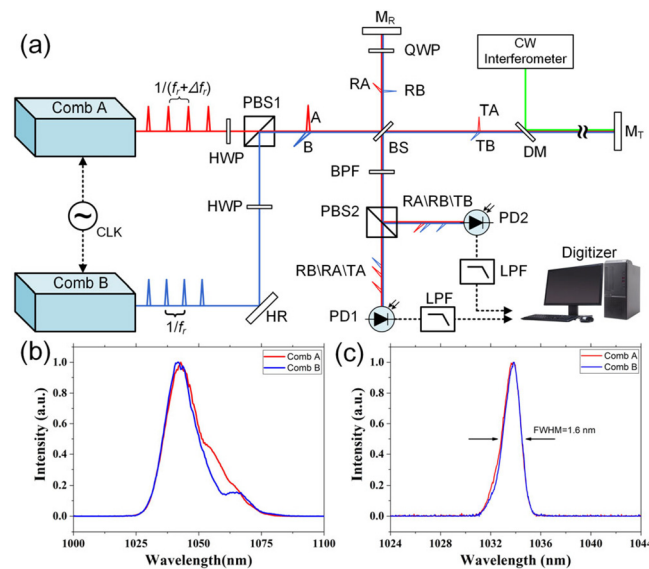


FIG. 1. (a) The experimental setup. HWP: half-wave plate, PBS: polarization beam splitter, BS: beam splitter, QWP: quarter wave plate, M_r : reference arm end mirror, M_t : target arm end mirror, DM: dichroic mirror, BPF: bandpass filter, PD: photodetector, and LPF: low-pass filter. (b) The spectra of combs A and B. (c) The spectra of combs A and B after the filter, with an FWHM of 1.6 nm.

These signal generators and frequency synthesizers generate reference frequencies for locking the repetition rates and carrier-envelope offset frequency. The carrier-envelope offset frequencies of two combs are locked to 20 MHz. The repetition rate of comb B was $f_{r,B}$ locked to 201.2 MHz, while that of comb A was $f_{r,A}$ locked to $201.2\ \text{MHz} + 5400\ \text{Hz}$. During the experiment, to achieve non-aliasing linear-optical sampling, we directly acquire a series of interferograms using a digitizer and then transform them into the frequency domain. If aliasing is detected, we adjust the repetition rate of comb A accordingly. Typically, adjusting the repetition rate from Hz to tens of Hz suffices to eliminate aliasing.

The pulses emitted by comb A ($f_r + \delta f_r$) and comb B (f_r) are combined using a polarization beam splitter (PBS). The combined pulses are then divided into two beams using a beam splitter (BS) and enter the target arms (labeled TA and TB, respectively) and reference arms (labeled RA and RB, respectively). The pulses reflected by two end mirrors are combined by BS and then divided into two paths via PBS2. As the pulses TA and TB are orthogonal, they are transmitted and reflected by PBS2, respectively. In the reference arm, there is a quarter-wave plate (QWP) that can be adjusted to ensure pulses RA and RB are both transmitted and reflected by the PBS2. The transmitted and reflected light pulses are received and converted into electrical signals. These signals are digitized by a two-channel 14-bit digitizer with a 200 M sampling rate, after being filtered through 100 MHz low-pass filters. The digitizer is synchronized to the rubidium clock.

In traditional dual-comb ranging schemes, there is typically one comb for distance measurement, serving as the signal comb, while the other comb performs asynchronous sampling and functions as the local oscillator comb. However, in the dual-comb ranging setup depicted in Fig. 1, both combs were used for distance measurement. The interferograms detected by PD1 and PD2 are shown in Fig. 2. The transmitted signal in Fig. 2(a) consists of RB, RA, and TA, where comb B is the local oscillator comb and comb A is the signal comb. By

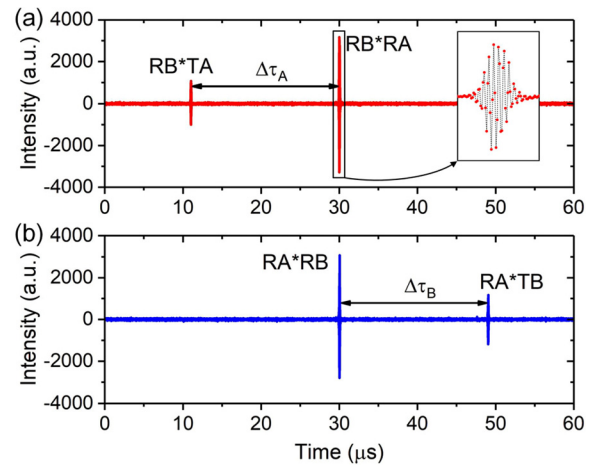


FIG. 2. (a) The time-domain interferograms of PD1. Comb A is the signal comb, and comb B is the local oscillator comb. The delay between reference interferograms $RB*RA$ and target interferogram $RB*TA$ is $\Delta\tau_A$. The inset provides a zoomed-in view of one reference interferogram $RB*RA$. (b) The interferograms of PD2 in the time domain. In this case, comb A is the local oscillator comb and comb B is the signal comb.

appropriately adjusting the amplitudes of TA and TB, the reference interferogram RB*RA and the target interferogram RB*TA can be distinguished based on their respective intensity. By calculating the time interval $\Delta\tau_A$ between the reference interferogram RB*RA and the target interferogram RB*TA, the measurement distance L_A can be expressed as

$$L_A = \frac{c}{2n_g} \Delta\tau_A \frac{\delta f_r}{f_{r,A}}, \quad (1)$$

where δf_r is the repetition rate difference and $f_{r,A}$ is the repetition rate of comb A. The interferogram details of RB*RA are shown in the inset of Fig. 2(a).

Similarly, in Fig. 2(b), comb A serves as the local oscillator comb, while comb B functions as the signal comb. By calculating the time interval $\Delta\tau_B$ between the reference interferogram RB*RB and the target interferogram RB*TB, the measurement distance L_B can be expressed as

$$L_B = \frac{c}{2n_g} \Delta\tau_B \frac{\delta f_r}{f_{r,B}}, \quad (2)$$

where $f_{r,B}$ is the repetition rate of comb B. The measured distances L_A and L_B are equal to the absolute distance L_{abs} of the measured object only within the NAR. When the absolute distance exceeds the NAR, the absolute distance L_{abs} and the measured distances L_A and L_B can be expressed as

$$L_{\text{abs}} = m\Lambda_{\text{NARA}} + L_A, \quad (3)$$

$$L_{\text{abs}} = m\Lambda_{\text{NARB}} + L_B, \quad (4)$$

$$m = (L_A - L_B) / (\Lambda_{\text{NARB}} - \Lambda_{\text{NARA}}), \quad (5)$$

where m is a positive integer and $\Lambda_{\text{NARA}} = c/2n_g f_{r,A}$ and $\Lambda_{\text{NARB}} = c/2n_g f_{r,B}$ represent the NARs when combs A and B are employed as signal combs, respectively.

When obtaining signals simultaneously from PD1 and PD2, the target interferograms RB*TA and TA*TB are positioned on the left and right sides of the reference interferogram RB*RA (or RB*RB). There are always two mirrored target interferograms in each measurement. For the following demonstrations, we always select the target interferogram that is closer to the reference interferogram to calculate L_A and L_B . Subsequently, we employ formula (5) to calculate the value of m . If m is positive, we proceed to calculate the absolute distance L_{abs} using formulas (3) and (4). However, if m is negative, the absolute distance and m value can be expressed as follows:

$$L_{\text{abs}} = m\Lambda_{\text{NARA}} + (\Lambda_{\text{NARA}} - L_A), \quad (6)$$

$$L_{\text{abs}} = m\Lambda_{\text{NARB}} + (\Lambda_{\text{NARB}} - L_B), \quad (7)$$

$$m = (L_A - L_B) / (\Lambda_{\text{NARA}} - \Lambda_{\text{NARB}}) - 1. \quad (8)$$

In this case, we recalculate m using formula (8), and the recalculated m must be positive. Then, formulas (6) and (7) are utilized to determine the absolute distance L_{abs} .

According to the experimental setup shown in Fig. 1, we demonstrated the absolute distance measurement of a static target with $m=4$. The laboratory was maintained at a temperature of 22°C, humidity of 48%, and air pressure of 10 001.2 Pa. The refractive index of air was estimated using the Ciddor equation.²⁴ The repetition rate of comb B was $f_{r,B} = 201.2$ MHz, while that of comb A was

$f_{r,A} = 201.2$ MHz + 5400 Hz. The measured update time was about 185 μs , corresponding to a maximum NAR of approximately 27 km. Reducing the repetition rate difference can further increase the NAR. Figure 3(a) shows the L_A (red line), L_B (blue line), and absolute distance (black line) calculated for a measurement time of up to 1.2 s. Here, the envelope of the interferogram was obtained using the Hilbert transform, and the peak of the interferogram was corrected using Gauss fitting.⁹ In Fig. 3(b), the Allan deviation of L_A and L_B with different averaging times is presented. The Allan deviations are about 4 μm for 185 μs , and they drop to 200 nm at 0.1 s. Because the variance of distance measurement is smaller than the difference of NAR ($\Lambda_{\text{NARB}} - \Lambda_{\text{NARA}} = 20$ μm), the value of m can be determined. We measured the jitter of the value of m 30 times, with each measurement taking 3.7 ms (20 interferograms) and an interval of approximately 1 min. The value of m was observed to be stable between 4 ± 0.1 , shown in Fig. 3(c). Figure 4 shows the comparison between the dual-comb system and a CW laser interferometer with 500 ms averaging time. The absolute distance in Fig. 4 is the same as in Fig. 3, which is also 3.0249 m. The residuals range from -138 to 75 nm, which also includes distance jitter caused by the environment.

To verify the dynamic distance measurement capability of this scheme for moving targets, we placed the end mirror M_T on a linear displacement stage (Thorlabs, LTS300C/M). The end mirror moves

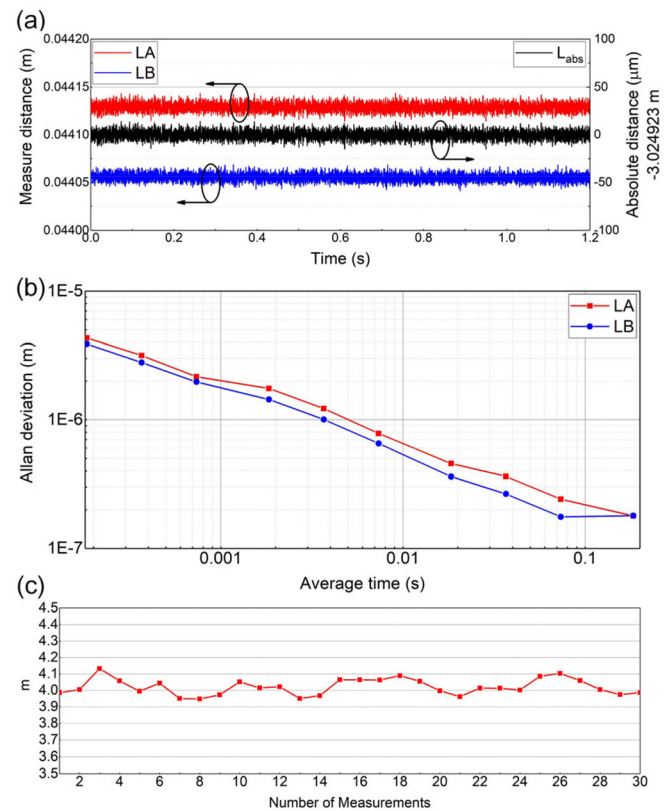


FIG. 3. (a) The absolute distance measurement of a static target. The left axis represents the measurement distance of L_A (red line) and L_B (blue line). The right axis represents the absolute distance (black line). (b) Allan deviation of L_A and L_B vs averaging time. (c) The jitter of the m value.

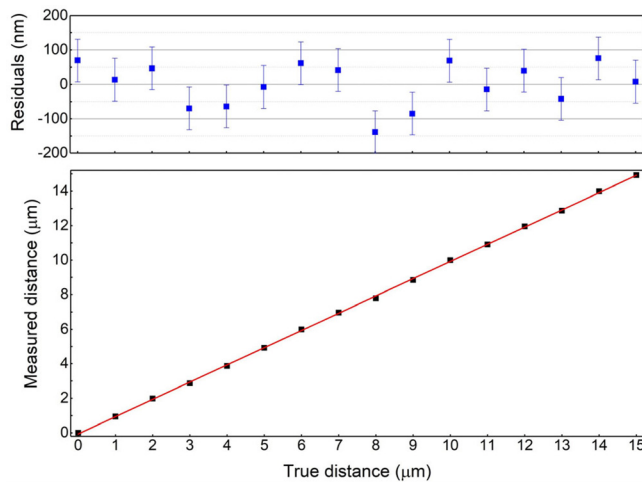


FIG. 4. Comparison between the distances measured vs a CW laser interferometer with an averaging period of 500 ms.

from 2.974 to 2.989 m, at a speed of 15 mm/s. Notably, 2.979 m is four times the NAR. The maximum speed of the target was limited by the translation stage. It is often challenging to achieve absolute distance measurement of a moving target using traditional methods of changing the repetition rate of signal comb, especially when the target's motion crosses an integer multiple of the NAR.

Figure 5(a) shows the changes in L_A and L_B throughout the measurement procedure. The difference in the repetition rate between combs A and B remains at 5400 Hz, resulting in an interferogram update time of 185 μ s. When the actual distance is less than 2.979 m, L_A is less than L_B , whereas when it exceeds 2.979 m, L_A surpasses L_B . The slopes of all four curves are identical and equal to the moving target's velocity. The insets provide specific details for two-time intervals, from 0.1 to 0.15 s and from 0.6 to 0.65 s, respectively. The dual-comb time-of-flight ranging technique is accomplished by calculating the time gap between the peak of the reference and the target interferograms. Nevertheless, in instances where the two interferograms overlap, accurately distinguishing their peaks to determine the distance becomes challenging, ultimately resulting in a measurement dead zone.¹¹ In the present configuration, the absolute distance of the dead zone is roughly $m \times \text{NAR} \pm 2$ mm, resulting in a measurement dead zone of approximately 4 mm. If the repetition rate difference decreases, the dead zone will diminish. Figure 5(b) shows the jitter of the m value. The value of m is calculated by averaging five interferograms, corresponding to 925 μ s update time. When the actual distance is less than 2.979 m, formula (8) is used to calculate m , while formula (5) is employed when the actual distance exceeds 2.979 m, here taking into account the selection of a target interferogram closer to the reference interferogram. Figure 5(c) illustrates the absolute distance of the moving target vs time, with an update rate of 925 μ s, similar to the previous figures. The graph demonstrates that even after passing through the dead zone, the correct distance can still be determined, and the intermediate discontinuity has no impact on the dual-comb distance measurement. Since we do not have a commercial interferometer that can perform moving targets, we use linear fitting to reflect the accuracy from a side view. The inset in Fig. 5(c) depicts the residual between the

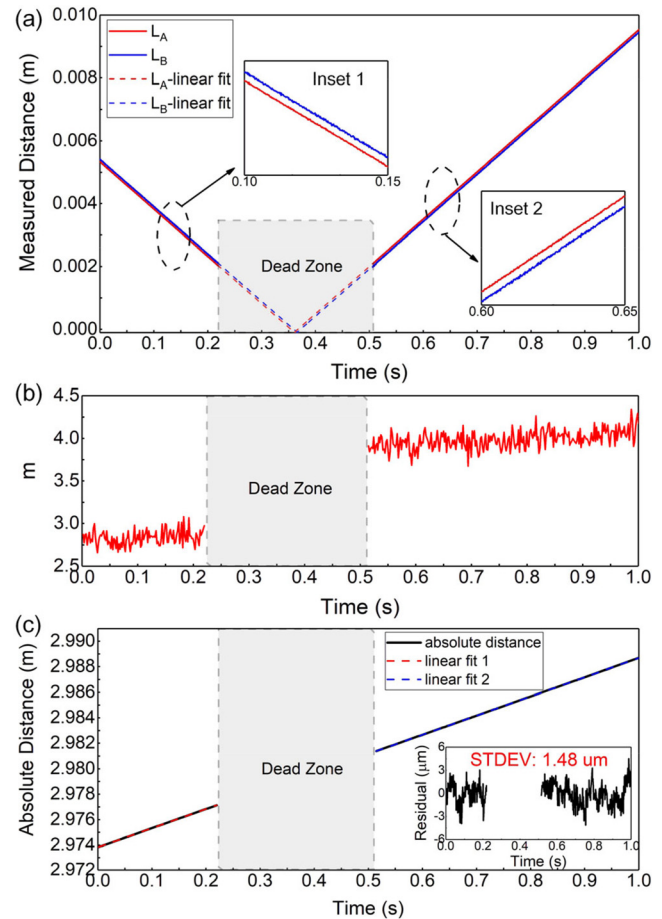


FIG. 5. Dynamic absolute distance measurement of moving target crossing dead zone. (a) The measurement distance of L_A and L_B . The update time is 185 μ s. The insets provide details for times ranging from 0.1 to 0.15 s and from 0.6 to 0.65 s. (b) The jitter of the m value. The value of m is calculated by averaging five interferograms (corresponding to 925 μ s update rate). (c) The absolute distance of the moving target vs time. Inset: the residual between the actual distance and the linear fit lines.

actual distance and the linear fit lines. The standard deviation of the residual is 1.48 μ m, which is due to both the jitter of the moving target and the jitter of the ranging.

In conclusion, we present a concise NAR extension dual-comb ranging scheme. By utilizing the polarization combining and splitting setting reasonably, this scheme enables simultaneous measurement of distance using the signal comb and the local oscillator comb in an interchanged manner. This scheme can extend the NAR to tens or even hundreds of kilometers. We demonstrated the absolute distance measurement of a static target using this setup, achieving a measurement precision of 4 μ m at 185 μ s averaging time and 180 nm at 0.18 s. Moreover, we performed dynamic measurements of the absolute distance of a moving target, crossing a dead zone of 3–4 times the NAR. The m value and absolute distance are obtained at an update time of 925 μ s. The standard deviation of the residual between the actual distance and the linear fit lines is only 1.48 μ m. This simple dual-comb ranging scheme does not require altering the repetition rate of the signal comb, active modulation, or the use of a tri-comb setup. With its

rapid, high precision, and ability to extend NAR, this absolute distance measurement scheme holds significant potential for various ranging applications in the future.

This study was supported by the Strategic Priority Research Program of the Chinese Academy of Sciences (Nos. XDA1502040404 and XDB2101040004) and the National Natural Science Foundation of China (NSFC) (No. 62305373).

AUTHOR DECLARATIONS

Conflict of Interest

The authors have no conflicts to disclose.

Author Contributions

Xiaodong Shao: Conceptualization (lead); Data curation (lead); Formal analysis (lead); Funding acquisition (supporting); Methodology (lead); Writing – original draft (lead). **Hainian Han:** Funding acquisition (lead); Project administration (equal); Supervision (equal); Writing – original draft (supporting); Writing – review & editing (equal). **Yu Yan:** Data curation (supporting); Formal analysis (supporting); Methodology (supporting). **Junyi Ma:** Formal analysis (supporting); Methodology (supporting). **Chengzhi Li:** Formal analysis (supporting); Methodology (supporting). **Zhiyi Wei:** Funding acquisition (supporting); Project administration (equal); Supervision (equal); Writing – review & editing (supporting).

DATA AVAILABILITY

The data that support the findings of this study are available from the corresponding author upon reasonable request.

REFERENCES

¹H.-C. Lim and H. Bang, *Acta Astronaut.* **65**(1–2), 112–122 (2009).

²H. Bosse and G. Wilkening, *Meas. Sci. Technol.* **16**(11), 2155 (2005).

³G. Peggs, P. G. Maropoulos, E. Hughes, A. B. Forbes, S. Robson, M. Ziebart, and B. Muralikrishnan, *Proc. Inst. Mech. Eng., Part B* **223**(6), 571–595 (2009).

⁴K. Minoshima and H. Matsumoto, *Appl. Opt.* **39**(30), 5512–5517 (2000).

⁵J. Ye, *Opt. Lett.* **29**(10), 1153–1155 (2004).

⁶K.-N. Joo and S.-W. Kim, *Opt. Express* **14**(13), 5954–5960 (2006).

⁷N. Schuhler, Y. Salvadé, S. Lévêque, R. Dändliker, and R. Holzwarth, *Opt. Lett.* **31**(21), 3101–3103 (2006).

⁸I. Coddington, W. C. Swann, L. Nenadovic, and N. R. Newbury, *Nat. Photonics* **3**(6), 351–356 (2009).

⁹T. A. Liu, N. R. Newbury, and I. Coddington, *Opt. Express* **19**(19), 18501–18509 (2011).

¹⁰H. Zhang, H. Wei, X. Wu, H. Yang, and Y. Li, *Opt. Express* **22**(6), 6597–6604 (2014).

¹¹J. Lee, S. Han, K. Lee, E. Bae, S. Kim, S. Lee, S.-W. Kim, and Y.-J. Kim, *Meas. Sci. Technol.* **24**(4), 045201 (2013).

¹²M.-G. Suh and K. J. Vahala, *Science* **359**(6378), 884–887 (2018).

¹³P. Trocha, M. Karpov, D. Ganin, M. H. Pfeiffer, A. Kordts, S. Wolf, J. Krockenberger, P. Marin-Palomo, C. Weimann, and S. Randel, *Science* **359**(6378), 887–891 (2018).

¹⁴Z. Zhu and G. Wu, *Engineering* **4**(6), 772–778 (2018).

¹⁵H. Zhang, H. Wei, X. Wu, H. Yang, and Y. Li, *Meas. Sci. Technol.* **25**(12), 125201 (2014).

¹⁶H. Zhang, X. Wu, H. Wei, and Y. Li, *IEEE Photonics J.* **7**(3), 1–8 (2015).

¹⁷D. R. Carlson, D. D. Hickstein, D. C. Cole, S. A. Diddams, and S. B. Papp, *Opt. Lett.* **43**(15), 3614–3617 (2018).

¹⁸J. Fellingner, G. Winkler, P. C. Aldia, A. S. Mayer, V. Shumakova, L. W. Perner, V. F. Pecile, T. Martynkien, P. Mergo, and G. Soboń, *Opt. Lett.* **46**(15), 3677–3680 (2021).

¹⁹X. Zhao, X. Qu, F. Zhang, Y. Zhao, and G. Tang, *Opt. Lett.* **43**(4), 807–810 (2018).

²⁰R. Li, X. Ren, B. Han, M. Yan, K. Huang, Y. Liang, J. Ge, and H. Zeng, *Opt. Lett.* **47**(20), 5309–5312 (2022).

²¹S. L. Camenzind, J. F. Fricke, J. Kellner, B. Willenberg, J. Pupekis, C. R. Phillips, and U. Keller, *Opt. Express* **30**(21), 37245–37260 (2022).

²²B. Martin, P. Feneyrou, D. Dolfi, and A. Martin, *Opt. Express* **30**(3), 4005–4016 (2022).

²³I. Coddington, N. Newbury, and W. Swann, *Optica* **3**(4), 414–426 (2016).

²⁴P. E. Ciddor and R. J. Hill, *Appl. Opt.* **38**(9), 1663–1667 (1999).